Broadband Stacked Microstrip Patch Antenna for L-Band Operation: FDTD Modeling

A. Hajiaboli*, F. Hodjat-Kashani* and M. Omidi*

Abstract: This paper presents a novel implementation of an electromagnetically coupled patch antenna using air gap filled substrates to achieve the maximum bandwidth. We also propose an efficient modeling technique using the FDTD method which can substantially reduce the simulation cost for modeling the structure. The simulated results have been compared with measurement to show the broadband behavior of the antenna and the accuracy of the proposed modeling technique. The measured results show a 16% of VSWR<2 bandwidth which is considerable considering the inherent bandwidth limitations in microstrip antenna technology.

Keywords: Broad Bandwidth, EMCP, FDTD Methods, Microstrip Antenna, Sub-cell Modeling.

1 Introduction

Achieving broadband behavior in microstrip antennas has always been challenging. Literature approves successful implementation of different broadbanding techniques such as multilayer stacked patches or air filled substrate.

In the method of air gap filled substrates an air gap is added to the substrate to reduce the dielectric constant of the feeding substrate [1]. This consequently reduces the quality factor and increases the bandwidth.

The proposed antenna structure considered in this paper is based on the combined these two broadbanding techniques to achieve the maximum bandwidth. The structure is an electromagnetically coupled patch antenna in which a thin air gap has been added beneath the feeding substrate to achieve the maximum bandwidth.

Electromagnetically coupled patch (EMCP) antenna was first introduced by Sabban in 1983 [2, 3]. The antenna is based on dual-layer stacked patches and because of its broadband behavior together with easy manufactured structure it has been under careful investigations until recently [4]-[10]. For example, Lee et. al. [4]-[6] experimented the effects of the parasitic patch sizes, dielectric superstartes and the distance between the patches on the behavior of the antenna very carefully.

Our numerical method to analysis the proposed antenna structure is finite-difference time-domain (FDTD) and since the thickness of the air gap is very thinner than the substrate the conventional FDTD girding can result to very small FDTD cells and consequently increases the computational burden.

To overcome this problem, we apply an efficient sub-cell modeling technique based on Maloney-Smith technique of thin dielectric sheets [11] to accurately simulate the antenna characteristics with acceptable computational burden. The simulated results have been compared with measured results to both show the broadband behavior and the effectiveness of the proposed modeling technique in FDTD.

2 The Antenna Structure

The conventional 3D view of the antenna structure is shown in Fig 1. The antenna is consisted of two patches placed in front of each other and separated with a spacer with dielectric constant of unity, e.g. a foam spacer.

To have a better understanding, a cross sectional view of the antenna structure inside the FDTD space is shown in Fig. 2. The patches are etched on a substrate with the dielectric constant of 3.38, loss-tangent of 0.0027, and thickness of 0.81mm. Another substrate with the same specifications is glued to the fed-patch to result in the total thickness of 1.75mm. The gap between these two substrates is considered as a thin air layer. Using this technique we both provide the appropriate thickness for the feeding substrate in the designed frequency and also reduce the effective dielectric constant of the feeding substrate. Reducing the effective dielectric constant reduces the quality factor and consequently increases the bandwidth.

The dimensions of the fed patch are Lx=64mm and Ly= 68mm, and the dimensions of the upper patch are Lx=72mm and Ly=72mm. The feed point is at x=10mm

Iranian Journal of Electrical & Electronic Engineering, 2007.
* The Authors are with the Department of Electrical Engineering. Iran universiy of Science and Technology, Narmak, Tehran, Iran.
E-mail: kashani@iust.ac.ir.

and y=4mm from the corner of the fed patch. The space between these patches is filled with a layer of foam spacer with the dielectric constant of unity (ε_r=1) which is considered as a varying thickness. Comparing the patch size the ground plane is finite and it is about 100mm×100mm. These dimensions are obtained using a moment method based commercial software (Microwave Office 2000) [12].

3 FDTD Simulation Space

A box of 90×90×60 cells is used as the FDTD space. The normal dimensions of the computational cells are chosen as $\Delta x=\Delta y=2$mm, $\Delta z=1.62$mm which are calculated using (1a). To achieve a better resolution near the feed-point and also near the dielectric layers, the graded mesh is applied. The cell dimensions for graded mesh are set in a way that the dimensions of each cell are not smaller than half of its adjacent cells. For example, for a one dimensional space the length of the ith cell should be between the following ranges $0.5\Delta l_{i\pm1} \le \Delta l_i \le 2\Delta l_{i\pm1}$ [13]. A 3D view of simulation space and it graded mesh is shown in Fig. 3. The Courant-stability condition which is given by (1b) resulted in $\Delta t=3.2\times10^{-12}$.

$$\Delta x, \Delta y, \Delta y < 1/10\lambda_0 \qquad (1a)$$

$$\Delta t < \frac{1}{C_0\sqrt{\frac{1}{\min(\Delta x)^2}+\frac{1}{\min(\Delta y)^2}+\frac{1}{\min(\Delta z)^2}}} \qquad (1b)$$

The absorbing boundary condition (ABC) which is used to minimize the reflected wave from the outer boundary is uniaxial perfectly matched layer (UPML) [13, 14]. The thickness of the UPML is 12 cells and $R(0)=e^{-16}$, which is the maximum reflection from the outer boundary. $\sigma_{x,max}=\sigma_{y,max}=3.77$ S/m , $\sigma_{z,max}=5$ S/m are calculated using (2) for x-directed axis.

$$R(\theta) = e^{-2\eta\sigma_{x,max}d\cos\theta/(m+1)} \qquad (2a)$$

$$\sigma_{x,max} = \frac{-(m+1)\ln[R(0)]}{2\eta d} \qquad (2b)$$

$$m = 3.75, d = 12\times\Delta x \qquad (2c)$$

$$k_{x,max} = k_{y,max} = k_{z,max} = 20 \qquad (2d)$$

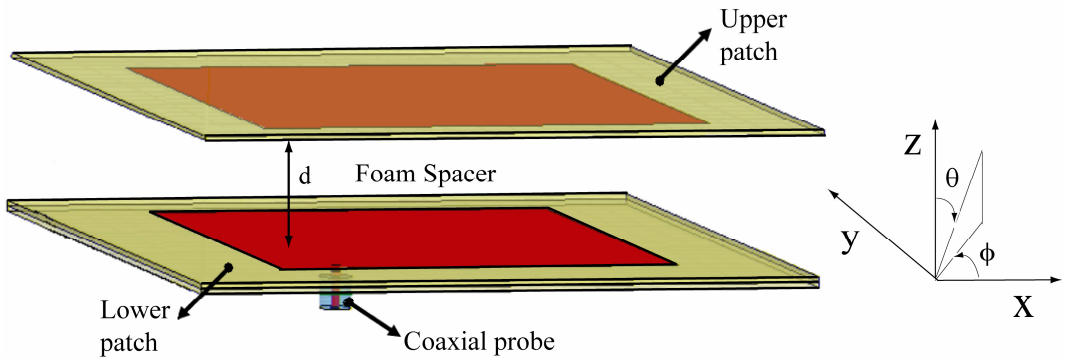

Fig. 1 3D view of the antenna.

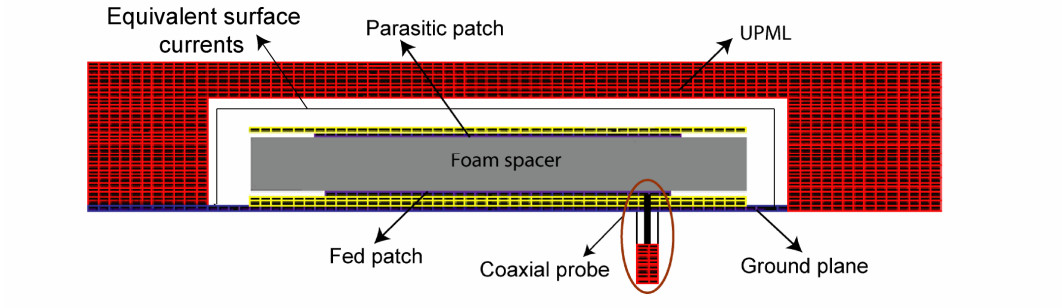

Fig. 2 Cross-section of the antenna inside the FDTD space.

Polynomial grading functions, as shown in (3) for x-directed axis, are used for grading the UPML. That means further going inside the boundary layers the losses will increase exponentially [13].

$$\sigma_x(x) = (x/d)^m \sigma_{x,max} \tag{3a}$$

$$k_x(x) = 1 + (k_{x,max} - 1).(x/d)^m \tag{3b}$$

To reduce the computational burden an infinite ground plane is chosen to truncate the bottom side of the simulation space as shown in Fig. 2.

4 Coaxial Probe-Fed Model

The coaxial fed model and its specifications are shown in Fig. 4. The accuracy of input impedance depends on the level of discretization used in FDTD method as shown in Fig. 5 [15]. The coaxial probe fed consisted of an inner conductor with diameter of 1mm and an outer conductor with diameter of 5mm. For satisfying the intrinsic impedance of Z_0=50Ω the space between these two conductors is filled with dielectric constant of ε_r=3.73.

The excitation signal is a Gaussian pulse modulated by a sinusoidal signal as given by

$$V_{exc}(n\Delta t) = e^{-\delta\times(n\Delta t - t_0)^2} \times \sin(\omega_0(n\Delta t - t_0))$$
$$t_0 = 4.6545\times10^{-10}, \delta = 10^{10}, \omega_0 = 3\pi\times10^9 \tag{4}$$

Here, δ is set to provide the desired frequency band for the simulation. t_0 must be chosen in a way that the casualty of the input signal be preserved. The excitation points shown in Fig. 5 are all excited simultaneously. The relationship between the excitation voltage and the excited electrical field is according to

$$V_{exc}(n\Delta t) = -E_z^n(i_f, j_f, k_f, +½)\Delta z \tag{5}$$

Input current is computed based on the quantization of Ampere's law which is integrated on a closed path very close to the inner conductor of the coaxial probe as the dashed line shows in Fig. 5. Input voltage is calculated according to the line integration of electric field at the coax to antenna transition.

The updating equations at the FDTD cell containing the thin air gap are based on a sub-cell modeling technique developed by Maloney and Smith [11]. In this method the normal component of the electric field is split into two separate components because of the discontinuity that occurs at the interface of the thin air gap with the substrate. These two components are updated using two separate FDTD updating equations. The other updating equations are updated considering this discontinuity and applying the average values of ε and σ instead of the values assessed by the dielectric substrate. The detail formulation of this technique can be found in [11] and [13].

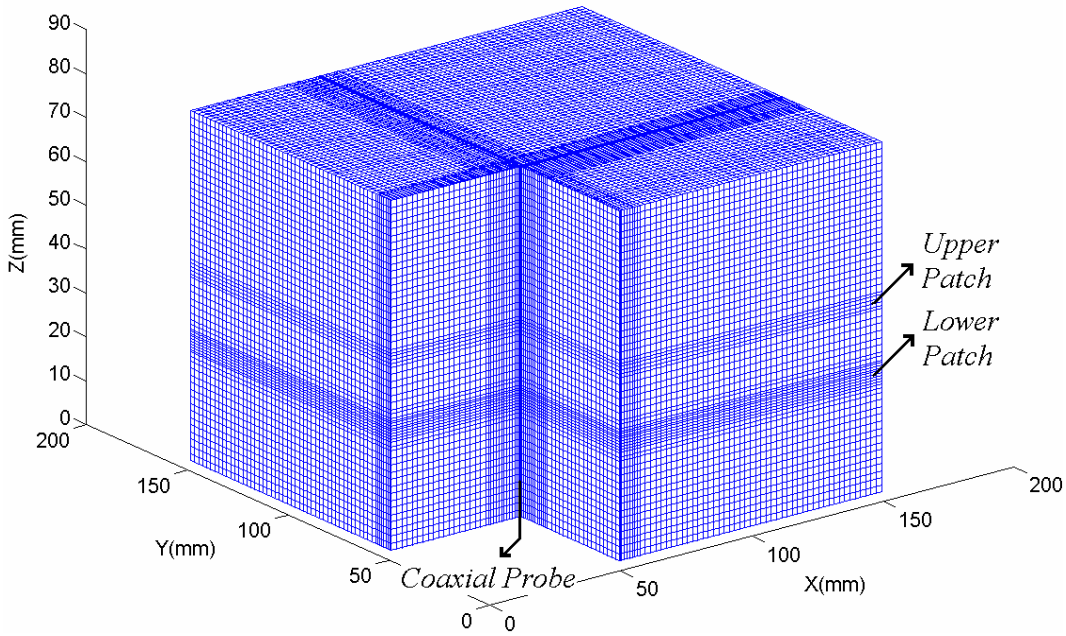

Fig. 3 3D view of the FDTD space.

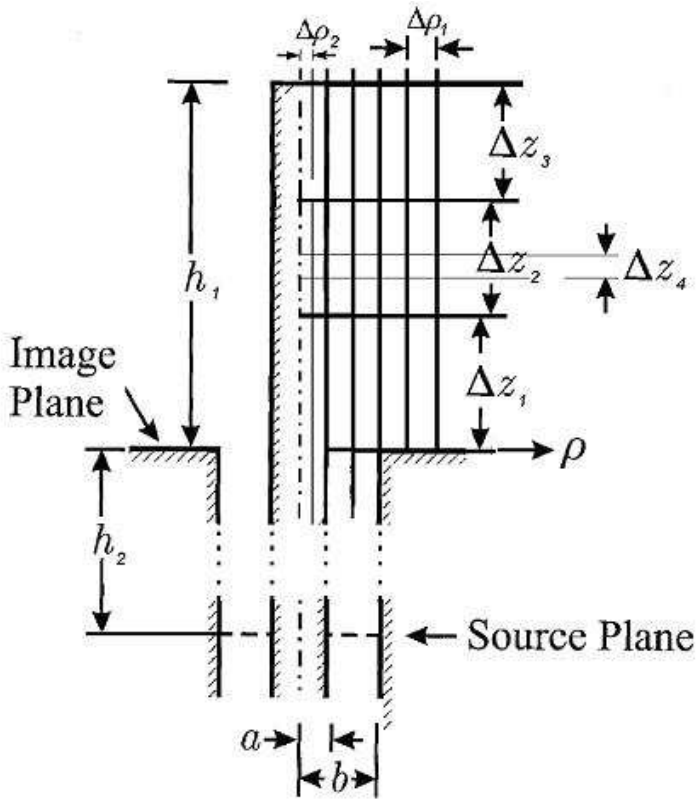

Fig. 4 Coaxial probe fed model ΔZ_4 corresponds to thin air gap.
$a = 0.5$mm, $b = 2.5$mm, $h_1 = 1.75$mm, $h_2 = 4$mm, $\Delta Z_1 = 0.61$mm, $\Delta Z_2 = 0.53$mm, $\Delta Z_3 = 0.61$mm, $\Delta Z_4 = 0.13$mm,
$\Delta\rho_1 = 0.5$mm, $\Delta\rho_2 = 0.25$mm

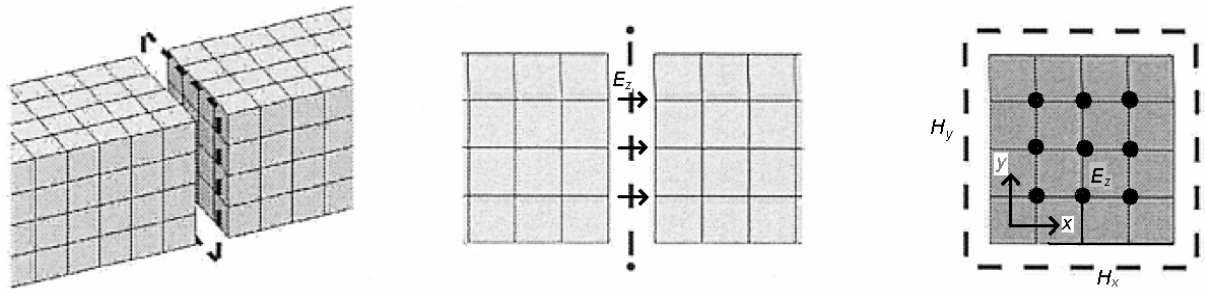

Fig. 5 Discretization of inner conductor of coaxial probe.

5 FDTD Simulation Results and Comparison with Measurements

Fig. 6 shows the measured VSWR for d=22mm. The bandwidth of VSWR<2 is about 16% at the center frequency of 1.36GHz. In the FDTD simulation, input impedance is calculated using (6).

$$Z_{in}(\omega) = \frac{V_{in}(\omega)}{I_{in}(\omega)} \qquad (6)$$

Fig. 7 and Fig. 8 show the measured and simulated real and imaginary parts of input impedance when d=18mm. A good similarity can be observed between the measured results and simulated results. As it is discussed in [15], if the discretization is smaller a better accuracy can be achieved. However, smaller cells cause more time consuming simulation.

6 Far Field Radiation Patterns

For calculating the far field, a time domain near to far field transformation is applied [13]. The far field components are calculated from the equivalent electric

and magnetic currents on the surface defined on the second layer inside the absorbing boundary layer as shown in Fig.2 that means: calculating $\vec{J}_s = \hat{n} \times \vec{H}_1$, $\vec{M}_s = -\hat{n} \times \vec{E}_1$ where $\hat{n}$ is the outward unit normal vector and $\vec{H}_1, \vec{E}_1$ are the magnetic and electric fields on the surface. $\Delta\theta = \pi/10$ and the total points to cover $0° \le \theta \le 180°$ are 11 points in each of $\phi = 90°$, $\phi = 0°$ planes. Smaller values of $\Delta\theta$ can give better resolution for radiated pattern. However, this makes the simulation more time consuming. Figs. 9 and 10 show the measured and simulated patterns at $\phi = 90°$, $\phi = 0°$ respectively.

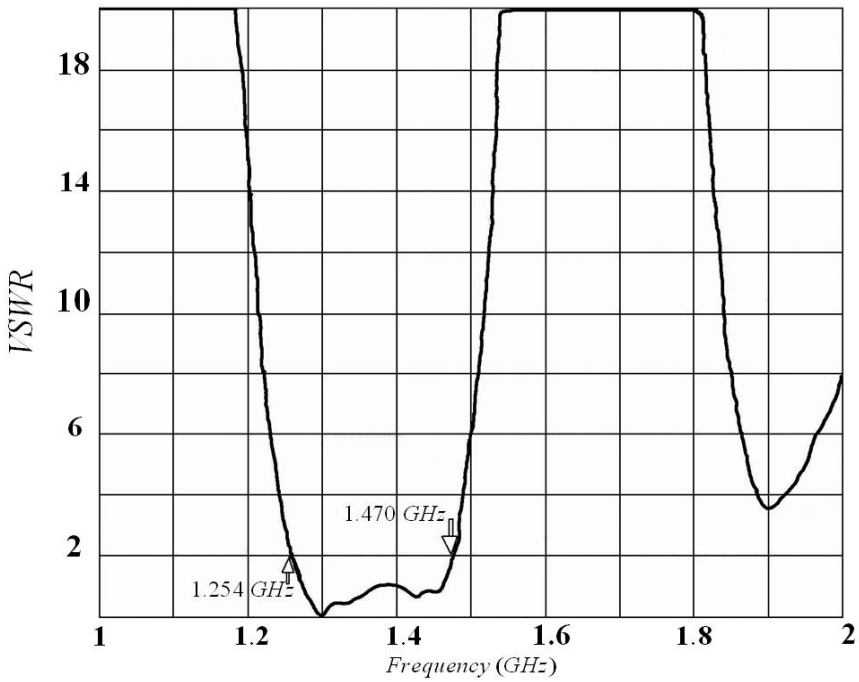

Fig. 6 VSWR versus frequency at d=22mm.

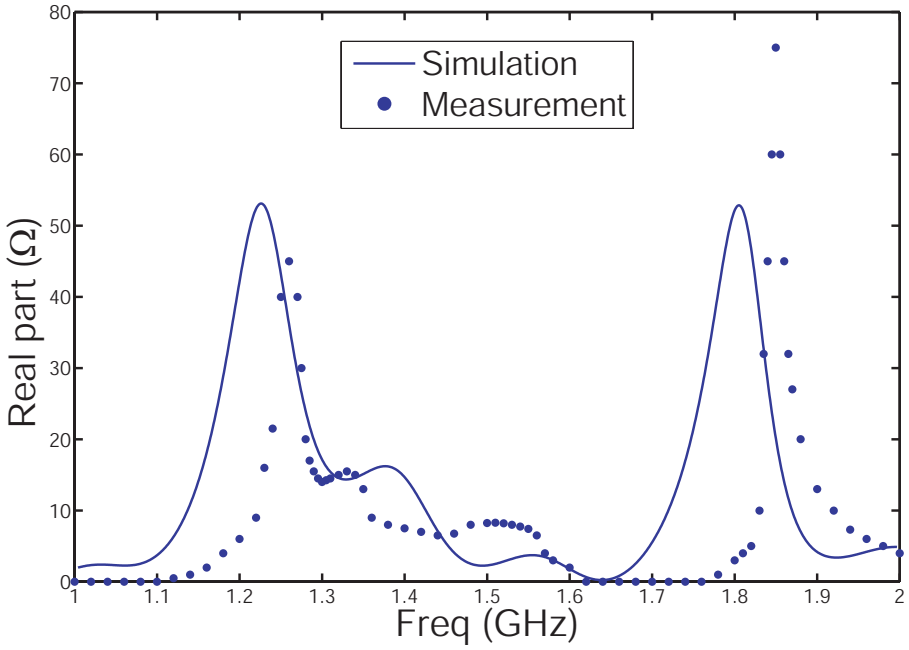

Fig. 7 Real part of input impedance at d=18mm.

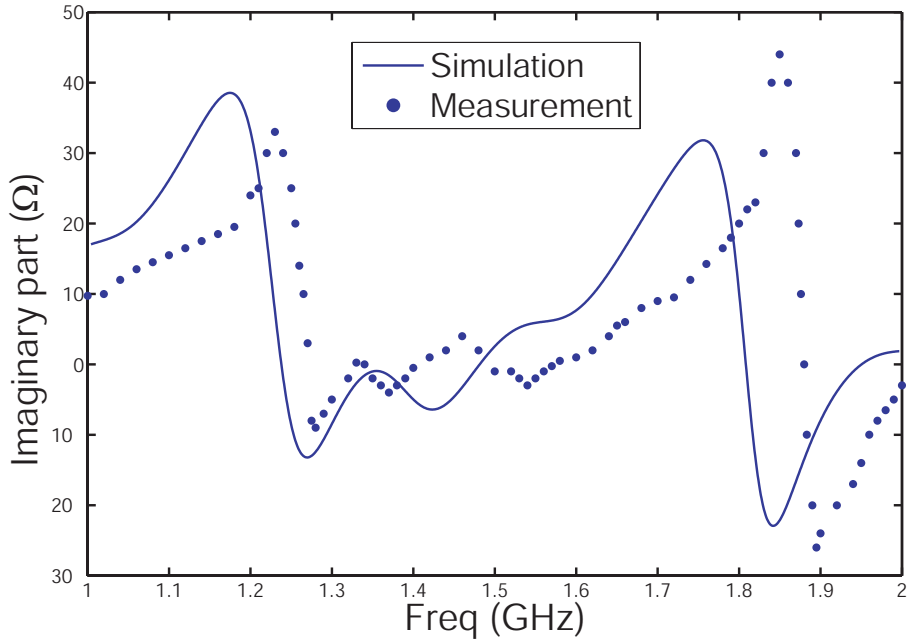

Fig. 8 Imaginary part of input impedance at d=18mm.

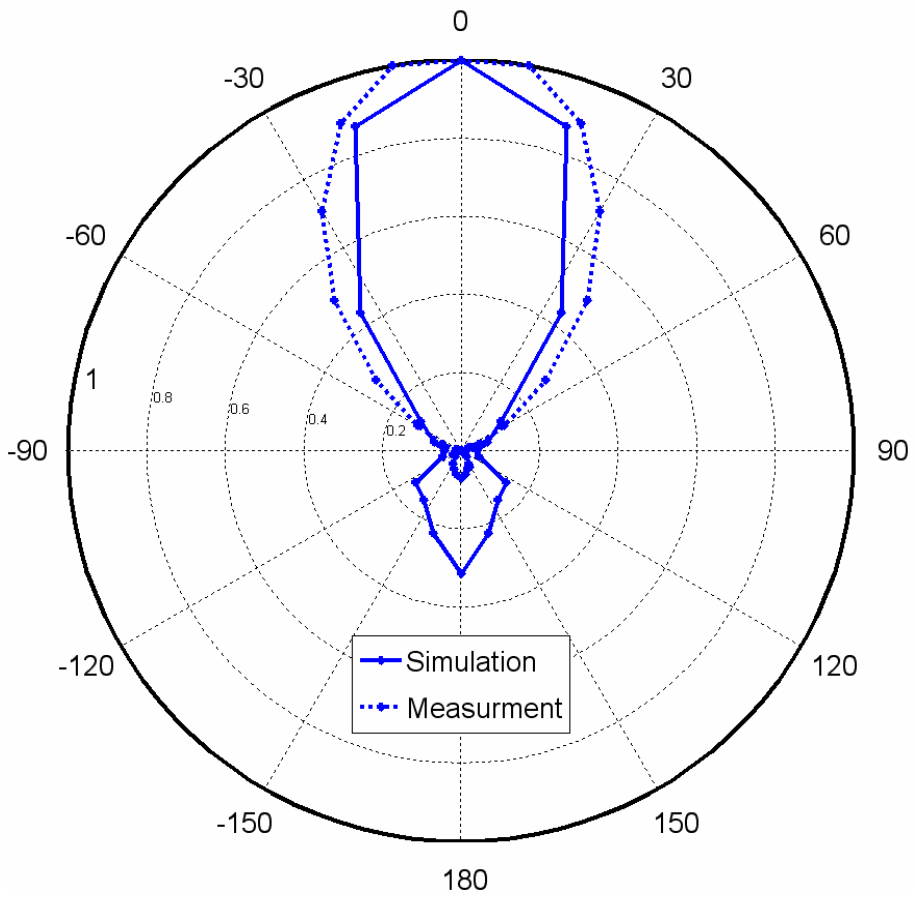

Fig. 9 Normalized Radiation pattern at $\phi = 90°$ measurement at 1.3GHz and simulation pattern at 1.23GHz. The difference is because of the difference in simulated resonance frequency and the measured one.

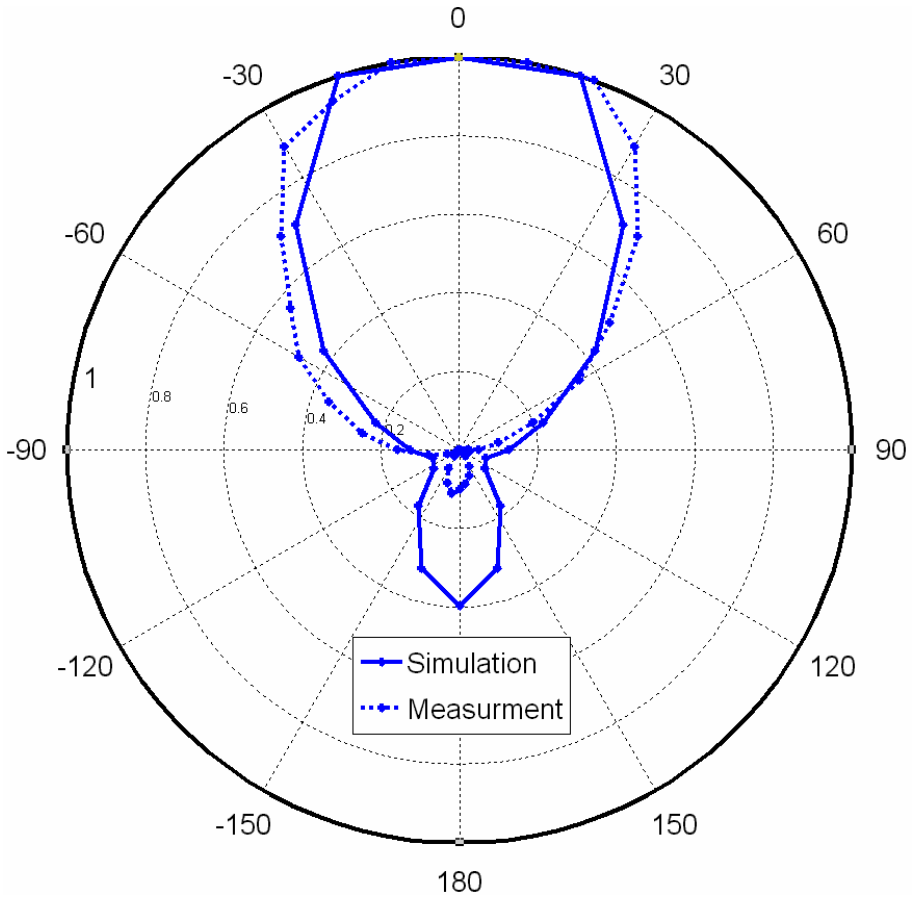

Fig. 10 Normalized Radiation pattern at $\phi = 0°$ measurement at 1.3GHz and simulation pattern at 1.23GHz. The difference is because of the difference in simulated resonance frequency and the measured one.

It should be noted that since there is a difference between the resonance frequency obtained in measurement and the one obtained by FDTD, the patterns are not shown at the same frequency. However, since the antenna is a microstrip type antenna it is expected that radiation won't changes dramatically by frequency. The measured beam-widths are about 110°, 75° at $\phi = 90°$, $\phi = 0°$ planes respectively. The measured front to back lobe ratio is -12dB and -11dB at $\phi = 90°$, $\phi = 0°$ respectively. The simulated front to back lobe is relatively larger than the measured one and this is in accordance with the results obtained in [10]. The reason for this may be because of outer boundary reflection.

The measured back lobe is relatively larger than what is obtained in single patch radiator. As discussed in [10], in this antenna the electromagnetic field from the fed patch reflects at the parasitic patch and the standing wave occurs between the fed patch and the parasitic patch. Since the reflected field at the parasitic patch radiates backward, the back lobe level increases.

7 Conclusion

A novel implementation of electromagnetically coupled patch antenna using air gap filled substrate has been studied with the aid of FDTD method. The thin air gap has been modeled using Maloney-Smith sub-cell modeling technique for thin material sheets to avoid time consuming simulation. The comparison of the measured input impedance with the simulated results based on FDTD approves the accuracy of the model. The measured bandwidth of the antenna at 1.36GHz is about 16% which is a broadband behavior considering the inherent bandwidth limitations in microstrip antennas. The input impedance shows that the broadband behavior is the result of simultaneous excitation of two modes which have almost the same resonance frequency [16]. A near to far field transformation has been applied to obtain the far field patterns. A good similarity between the measured beamwidths and simulated beamwidths has been observed but the simulated front to back lobe ratio is relatively larger than the measured values and this may be due to the outer boundary reflection. The beamwidths are about 110° and 75° and the measured front to back lobe ratio is -11dB and -12dB at $\phi = 90°$, $\phi = 0°$ respectively. Although the finite ground plane has some effects on the measured large back lobe level, the main reason for that, as discussed in [10], is the reflected wave from the parasitic patch.

References

[1] Kumar G. and Ray K. P., *Broadband microstrip antennas*, Artech House Inc., 2003.

[2] Sabban A., "A new broadband stacked two-layer microstrip antenna," *IEEE Antennas Propagat. Symp. Digest*, Vol. 21, pp. 63-66, May 1983.

[3] Johnson, R. C. and Jasik H., *Antenna Engineering Handbook*, 2nd ed., McGraw-Hill, Inc., NY,1984.

[4] Lee, R. Q. and Lee K. F., "Experimental study of two-layer electromagnetically coupled rectangular patch antenna," *IEEE Trans. on Antennas and Propagat.*, Vol. AP-38, No.8, pp. 1298–1302, Aug.1990.

[5] Lee R. Q. and Lee K. F., "Effects of parasitic patch sizes on multi-layer electromagnetically coupled patch antenna," *IEEE. Antennas and Propagat. Symp. Digest*, Vol. 27, pp. 624-627, June 1989.

[6] Lee R. Q., Zaman A. J., and Lee K. F., "Effects of dielectric superstrates on a two-layer electromagnetically coupled patch antenna," *IEEE Antennas and Propagat. Symp. Digest*, Vol. 27, pp. 620-623, June 1989.

[7] Fan Z. and Lee K. F., "Input impedance of electromagnetically coupled patch antennas," *IEEE Antennas and Propagat. Symp. Digest*, pp. 1935-1938, July 1992.

[8] Chung K. L. and Mohan A. S., "A Broadband Singly-Fed Electromagnetically Coupled Patch Antenna for Circular Polarization," *Proc WARS02, Workshop on the Application of Radio Science*, Sydney, Australia, Feb. 2002.

[9] AL-Charchafchi S. H., and Loukrezis F. M., "Electromagnetically coupled stacked microstrip patch antennas," *Microwave Journal*, Vol. 38, No. 6, P76 (3), June 1995.

[10] Nishiyama E., Aikawa M. and Egashira S., "FDTD Analysis of Stacked Microstrip Antenna With High Gain," *Progress in Electromagnetics Research, (PIER)*, Vol. 33, pp. 29–43, 2001.

[11] Malonet J.G., Smith G. S., "The efficient modeling of thin material sheets in the FDTD method," *IEEE trans. Antennas and Propagat.* Vol. 40, pp.323-330, 1992.

[12] Hajiaboli A., Hojjat-Kashani F., "FDTD Simulation of an Inverted Patch Stacked Microstrip Antenna," *International Symposium on Telecommunications, IST2003*, Isfahan, Iran, August 2003.

[13] Taflove A., *Computational Electrodynamics: The Finite-Difference Time-Domain Method*, Artech House Inc., 1995.

[14] Berenger J.-P., "Three-Dimensional Perfectly Matched Layer for the Absorption of Electromagnetic Waves," *Journal of Computational Physics*, Vol. 127, pp. 363–379, 1996.

[15] Hertel Th. W., Smith G. S., "On the Convergence of Common FDTD Feed Models for Antennas," *IEEE Tran. on Antennas and Propagat.*, Vol. 51, No. 8, August 2003.

[16] Zucher J. F. and Gardiol F. E., *Broadband Patch Antennas*, Artech House Inc.,1995.

Amir Hajiaboli obtained the B.Sc. from University of Tehran in 2000 and the M.Sc. with highest distinction from Iran University of Science and Technology in 2003 both in electrical engineering. Since Sept. 2004 he has been pursuing his Ph.D. in electrical engineering with the Department of Electrical and Computer Engineering at McGill University in Montreal Canada. His research interests focus on computational electromagnetic for antennas and bio-medical applications. He has extensive experiences in developing computational electromagnetic codes using finite-difference time-domain method. He is currently working on simulating the electrodynamics of light interaction with retinal photoreceptors.

Farokh Hodjat-Kashani received his Ph.D. in Electrical Engineering specializing in Electromagnetics from the University of California at Los Angeles in 1970. From 1970 to 1971 he was an Assistant Prof at Higher Institute of Telecommunication and University of Tehran. From 1971 to 1976 he was an Assistant Prof. and chairman of E. E. Dept. at IUST and from 1976 to 1977 spent sabbatical leave in Hughes Aircraft Company, aerospace division at Canoga Park, California, US. From June 1987 to June 1988 he took one year sabbatical leave in Communication Department, New South Wales University, Sydney, Australia. He is currently a Professor of Electrical Engineering Department, Iran University of Science and Technology. In April 2002 he was selected as an outstanding professor in Iran. He has published over sixty papers and twelve books in Persian.

Mohammad Omidi photograph and biography not available at the time of publication.